Supporting Information for

Coordination-driven Assembly of Dysprosium Layers into Framework Featuring Enhanced Energy Barrier and Quantum Tunneling of Magnetization

Zhen-Na Huang, ‡[a] Rong Sun, ‡[b] Fang Ma,[a] Jing Yang,[a] Xiao-Xiao Huang, [c] Hao-Ling Sun,*[a] and Song Gao*[b]

[a] *Department of Chemistry and Beijing Key Laboratory of Energy Conversion and Storage Materials, Beijing Normal University, Beijing 100875, P. R. China. E-mail: haolingsun@bnu.edu.cn;*

[b] *Beijing National Laboratory for Molecular Sciences, State Key Laboratory of Rare Earth Materials Chemistry and Applications, College of Chemistry and Molecular Engineering, Peking University, Beijing 100871, P. R. China. E-mail: gaosong@pku.edu.cn;*

[c] *Department of physics, Beijing Normal University, Beijing 100875, P. R. China.*

‡ These authors contributed equally.

X-ray crystallography and physical measurement

Intensity data for crystals of **1** and **2** were collected on a rigaku SuperNova, Dual, AtlasS2 diffractometer with graphite-monochromated Mo Kα (λ = 0.71073 Å) radiation at 100 K. Using Olex2, the structure was solved with the olex2.solve structure solution program using Charge Flipping and refined with the olex2.refine refinement package using Gauss-Newton minimisation. All non-hydrogen atoms were refined anisotropically. Hydrogen atoms were placed at the calculation positions. The details of crystallographic data and selected bond parameters for compounds **1** and **2** are listed in Table S1†, Table S2† and Table S3†, respectively. CCDC 2243064-2243065 contain the supplementary crystallographic data for this paper.

The Fourier transform infrared (FT-IR) spectra were recorded using KBr pellets in the range of 4000 to 400 cm^{-1} on an AVATAR 360 Nicolet 380 FT/IR spectrometer. Elemental analyses (C, H, N) were implemented on an Elementar Vario EL analyzer.

Powder X-ray diffraction (PXRD) analyses were performed on a Rigaku Dmax-2000 X-ray diffractometer with Cu Kα (λ=1.54059 Å) radiation. Variable-temperature magnetic susceptibility measurements of **1** and **2** were performed on Quantum Design PPMS magnetometer (100~10000 Hz) and Quantum Design SQUID-MPMS3 (1~1000 Hz) magnetometer. Prior to magnetic experiment, the crystal sample was encapsulated with film and fixed in an antimagnetic capsule and then placed in a sample holder for testing.

Computational details

Ab initio calculations on the Dy^{3+} ion fragment of compound **1** and **2** on the basis of X-ray determined geometry have been carried out with MOLCAS 8[1] program package. Since the two Dy^{3+} ions of the dimer units are structurally identical, only calculation based on one of the Dy^{3+} ions were conducted. The method is to retain one Dy^{3+} ion while replacing the other with a diamagnetic Lu^{3+} ion without further optimization.

The basis sets for all atoms are atomic natural orbitals from the MOLCAS ANO-RCC library: ANO-RCC-VTZP for Dy^{3+} ion; VTZ for close O and N; VDZ for distant atoms. The calculations employed the second order Douglas-Kroll-Hess Hamiltonian, where scalar relativistic contractions were taken into account in the basis set and the spin-orbit coupling were handled separately in the restricted active space state interaction (RASSI-SO) procedure. For the fragment of Dy^{3+} ion, the active electrons in 7 active spaces include all f electrons CAS (9, 7) for Compound **1** and **2** in the CASSCF calculation. To exclude all the doubts, we calculated all the roots in the active space. We have mixed the maximum number of spin-free state which was possible with our hardware (all from 21 sextets, 128 from 224 quadruplets and 130 from 490 doublets for Dy^{3+} ion fragments).

Fitting the exchange interaction in two compounds using Lines model based on *ab initio* results

With the corresponding calculated results of the mononuclear fragments, the magnetic interactions were further explored. The exchange interaction J_{exch} between the magnetic centers is considered within the Lines model, while the account of the dipole-

dipole magnetic coupling J_{dip} is treated exactly. The J_{exch} could be described with Hamiltonian S1 shown below. The Lines model is effective and has been successfully used widely in the research field of f-element single-molecule magnets.

$$\hat{H}_{exch} = -J_{exch} \hat{S}_{Dy1} \hat{S}_{Dy1A} \quad \text{(S1)}$$

$$J_{dip} = \frac{\mu_0 \mu_B^2}{4\pi |r|^3} g_{1z} g_{2z} (1-3\cos^2\theta) \quad \text{(S2)}$$

$$J_{total} = J_{dip} + J_{exch} \quad \text{(S3)}$$

The $\hat{S}_{Dy} = \pm 1/2$ are the ground pseudospin on the Dy^{3+} ion sites. The J_{dip} parameters can be calculated exactly on account of the X-ray determined molecular structures using the eqn (S2), where $|r|$ was the distance between two Dy^{3+} ions and θ was the angle between the r vector and magnetic easy axis. The J_{exch} was fitted through comparison of the computed and measured magnetic susceptibility and molar magnetization using the POLY_ANISO program.[2]

Table S1. Crystallographic Data and Structure Refinement for compounds **1** and **2**.

	1	**2**
Formula	$C_{15}H_{22}ClDyN_4O_{11}$	$C_{22}H_{20}ClDyN_6O_{11}$
Mr	632.32	742.39
Crystal system	monoclinic	monoclinic
Space group	*P2₁/c*	*C2/c*
a (Å)	12.4752(5)	26.0881(6)
b (Å)	15.9061(5)	14.2365(3)
c (Å)	11.2332(4)	14.9743(4)
a (°)	90.00	90.00
β (°)	106.660(4)	102.922(2)
γ (°)	90.00	90.00
V (Å^3)	2135.45(13)	5420.7(2)
Z	4	8
μ (mm^{-1})	3.690	2.925
F (000)	1244.0	2920.0
GOF	1.058	1.061
Data collected	16731	19837
Unique	3763	6347
R_{int}	0.0489	0.0491
*R*1, *wR*2 [$I > 2\sigma(I)$]	0.0416, 0.0934	0.0396, 0.0946
R1, wR2 [all data]	0.0493, 0.0971	0.0582, 0.1023

Table S2. Selected Bond Distances (Å) and Bond Angles (°) in compounds **1** and **2.**

1		**2**	
Dy-O1	2.150	Dy-O1	2.161
Dy-O2	2.351	Dy-O2	2.317
Dy-O2A	2.340	Dy-O2A	2.392
Dy-O3	2.353	Dy-O3	2.359
Dy-O4	2.372	Dy-O4	2.414
Dy-O5	2.420	Dy-O5	2.321
Dy-N1	2.488	Dy-N1	2.480
Dy-N3	2.580	Dy-N3	2.580
O1-Dy-O2	137.643	O1-Dy-O2	139.677
O1-Dy-O2A	153.053	O1-Dy-O2A	143.883
O1-Dy-O3	85.943	O1-Dy-O3	84.520
O1-Dy-O4	100.961	O1-Dy-O4	80.010
O1-Dy-O5	85.808	O1-Dy-O5	113.495
O1-Dy-N1	74.135	O1-Dy-N1	74.613
Dy-O2-Dy	113.752	Dy-O2-Dy	112.084

Table S3. Hydrogen Bonds and Weak Interaction in **1**.

D-H	d(D-H) (Å)	<DHA(°)	d(D…A) (Å)	A
O3-H3A	0.89	125.2	2.208	O10
O3-H3B	0.89	130.9	2.600	O11
O10-H10	0.84	158.9	2.954	O7 (+X, 1/2-Y, -1/2+Z)
O5-H5	0.86	156.6	2.908	O9 (1-X, 1/2+Y, 3/2-Z)
C15-H15	0.95	134.2	3.278	O7 (1+X, 1/2-Y, -1/2+Z)

Table S4. Hydrogen Bonds in **2**.

D-H	d(D-H) (Å)	<DHA(°)	d(D…A) (Å)	A
O8-H8A	0.87	176.1	2.868	O11

Table S5. The CShM values calculated by SHAPE 2.0 for **1** and **2**.

Coordination Geometry	**1**	**2**
Octagon (D_{8h})	31.615	31.688
Heptagonal pyramid (C_{7v})	23.484	22.350
Hexagonal bipyramid (D_{6h})	14.473	16.429
Cube (O_h)	11.818	11.536
Square antiprism (D_{4d})	3.589	2.434
Triangular dodecahedro (D_{2d})	2.010	1.770
Biaugmented trigonal prism (C_{2v})	2.714	1.536
Triakis tetrahedron (T_d)	12.617	11.959
Elongated trigonal bipyramid (D_{3h})	22.161	20.417

Table S6. Relaxation fitting parameters from Least-Squares Fitting of $\chi(f)$ data under zero dc field of **1**.

T/K	χ_T	χ_s	α	τ
5	2.858	0.022	0.229	0.4105
5.5	2.693	0.021	0.226	0.2936
6	2.473	0.020	0.217	0.1973
6.5	2.354	0.019	0.216	0.1420
7	2.230	0.017	0.217	0.1019
7.5	2.103	0.016	0.216	0.0722
8	1.973	0.014	0.214	0.0510
8.5	1.860	0.012	0.215	0.0366
9	1.742	0.012	0.212	0.0260
9.5	1.645	0.010	0.211	0.0189
10	1.545	0.009	0.205	0.0139
10.5	1.457	0.009	0.199	0.0103
11	1.384	0.009	0.197	0.0078
11.5	1.310	0.010	0.120	0.0060
12	1.250	0.009	0.188	0.0046
12.5	1.189	0.010	0.183	0.0036
13	1.140	0.010	0.183	0.0028
13.5	1.090	0.012	0.179	0.0023
14	1.045	0.018	0.171	0.0018
14.5	1.008	0.020	0.172	0.0015
15	0.966	0.027	0.164	0.0012
15.5	0.934	0.033	0.163	9.61×10^{-4}
16	0.902	0.008	0.162	6.69×10^{-4}
17	0.846	0.009	0.178	4.26×10^{-4}
18	0.796	0.011	0.211	2.91×10^{-4}
19	0.851	0	0.340	2.11×10^{-4}
20	0.807	0	0.364	1.36×10^{-4}
21	0.762	0	0.379	9.37×10^{-5}
22	0.723	0.001	0.394	6.32×10^{-5}
23	0.687	0.020	0.404	4.44×10^{-5}

Table S7. Relaxation fitting parameters from Least-Squares Fitting of $\chi(f)$ data under zero dc field of **2**.

T/K	χ_T	χ_s	α	τ
2	19.311	0.076	0.364	2.2822
3	9.991	0.072	0.352	1.0053
4	6.088	0.072	0.328	0.4597
5	4.068	0.074	0.285	0.1842
5.5	3.430	0.074	0.259	0.1124
6	2.970	0.073	0.237	0.0698
6.5	2.619	0.073	0.215	0.0443
7	2.347	0.073	0.196	0.0291
7.5	2.139	0.072	0.183	0.0199
8	1.965	0.073	0.169	0.0139
8.5	1.822	0.073	0.161	0.0100
9	1.697	0.074	0.151	0.0073
9.5	1.591	0.074	0.145	0.0054
10	1.497	0.076	0.138	0.0041
10.5	1.413	0.079	0.132	0.0031
11	1.341	0.080	0.131	0.0024
11.5	1.274	0.084	0.125	0.0019
12	1.214	0.089	0.121	0.0015
12.5	1.162	0.092	0.122	0.0012
13	1.112	0.099	0.118	9.05×10^{-4}
13.5	1.066	0.106	0.115	7.21×10^{-4}
14	1.027	0.062	0.138	5.13×10^{-4}
14.5	0.988	0.063	0.139	4.01×10^{-4}
15	0.951	0.066	0.134	3.11×10^{-4}
15.5	0.919	0.067	0.135	2.42×10^{-4}
16	0.887	0.070	0.133	1.88×10^{-4}

16.5	0.858	0.073	0.132	1.46×10^{-4}
17	0.859	0.053	0.196	1.11×10^{-4}
17.5	0.831	0.054	0.196	8.61×10^{-5}
18	0.803	0.056	0.196	6.69×10^{-5}
18.5	0.778	0.057	0.195	5.20×10^{-5}
19	0.751	0.065	0.186	4.14×10^{-5}
19.5	0.731	0.066	0.187	3.27×10^{-5}
20	0.712	0.064	0.193	2.55×10^{-5}
20.5	0.691	0.067	0.191	2.03×10^{-5}
21	0.673	0.067	0.195	1.60×10^{-5}
21.5	0.652	0.102	0.165	1.43×10^{-5}

Table S8. Calculated energy levels (cm^{-1}) and $\boldsymbol{g}$ (g_x, g_y, g_z) tensors of the lowest Kramer doublets (KDs) of the Dy^{3+} fragments, and wavefunction composition for the eight Kramer doublets of the $^6H_{15/2}$ ground multiplet of compounds **1** and **2**.

KDs	**1**			**2**		
	E	***g***	m_J wave functions	*E*	***g***	m_J wave functions
1	0.0	0.00 0.00 19.60	95.2%|±15/2⟩ + 0.0%|±13/2⟩ + 4.5%|±11/2⟩ + 0.3%|±9/2⟩ + 0.0%|±7/2⟩	0.0	0.01 0.02 19.73	97.9%|±15/2⟩ + 0.0%|±13/2⟩ + 1.3%|±11/2⟩ + 0.6%|±9/2⟩ + 0.1%|±7/2⟩
2	230.0	0.05 0.07 16.90	0.4%|±15/2⟩ + 81.5%|±13/2⟩ + 5.2%|±11/2⟩ + 10.5%|±9/2⟩ + 1.9%|±7/2⟩	115.5	0.10 0.15 17.52	72.3%|±13/2⟩ + 19.7%|±11/2⟩ + 5.5%|±9/2⟩ + 0.9%|±7/2⟩ + 0.8%|±3/2⟩
3	410.2	1.79 3.48 14.99	16.0%|±11/2⟩ + 15.7%|±7/2⟩ + 13.1%|±5/2⟩ + 20.4%|±3/2⟩ + 24.5%|±1/2⟩	208.5	1.29 2.88 15.38	18.1%|±9/2⟩ + 12.5%|±7/2⟩ + 13.0%|±5/2⟩ + 17.3%|±3/2⟩ + 21.4%|±1/2⟩
4	455.4	1.70 3.61 9.79	7.0%|±13/2⟩ + 40%|±11/2⟩ + 10.6%|±5/2⟩ + 11.0%|±3/2⟩ + 17.4%|±1/2⟩	246.4	1.41 4.51 9.00	12.5%|±13/2⟩ + 28.8%|±11/2⟩ + 15.2%|±9/2⟩ + 10.5%|±7/2⟩ + 18.5%|±1/2⟩
5	556.9	8.53 6.85 4.55	17.0%|±11/2⟩ + 21.4%|±9/2⟩ + 7.8%|±7/2⟩ + 21.6%|±3/2⟩ + 9.8%|±1/2⟩	306.9	4.09 5.40 10.59	18.7%|±11/2⟩ + 20.1%|±7/2⟩ + 19.0%|±5/2⟩ + 16.7%|±3/2⟩ + 13.5%|±1/2⟩
6	606.3	0.19 2.84 13.82	16.7%|±9/2⟩ + 13.3%|±7/2⟩ + 14.9%|±5/2⟩ + 18.1%|±3/2⟩ + 29.2%|±1/2⟩	373.4	0.05 0.43 16.36	9.1%|±9/2⟩ + 15.2%|±7/2⟩ + 27.8%|±5/2⟩ + 25.5%|±3/2⟩ + 15.1%|±1/2⟩
7	638.3	1.14 1.83 17.92	20.0%|±9/2⟩ + 21.6%|±7/2⟩ + 15.6%|±5/2⟩ + 19.4%|±3/2⟩ + 16.4%|±1/2⟩	441.4	0.10 0.47 18.22	6.1%|±11/2⟩ + 7.2%|±7/2⟩ + 24.8%|±5/2⟩ + 28.3%|±3/2⟩ + 27.8%|±1/2⟩
8	714.2	0.04 0.14 19.30	6.2%|±11/2⟩ + 22.1%|±9/2⟩ + 33.7%|±7/2⟩ + 24.4%|±5/2⟩ + 9.5%|±3/2⟩ +	502.8	0.09 0.24 18.80	12.5%|±11/2⟩ + 36.1%|±9/2⟩ + 33.6%|±7/2⟩ + 10.1%|±5/2⟩ + 3.5%|±1/2⟩

Table S9. Fitted exchange coupling constant J_{exch}, the calculated dipole-dipole interaction J_{dip} and the total J between Dy^{3+} ions in **1** (cm^{-1}) and **2** (cm^{-1}).

		1	**2**
J	J_{dip}	4.6	4.8
	J_{exch}	-2.0	-1.5
	J_{total}	2.6	3.3

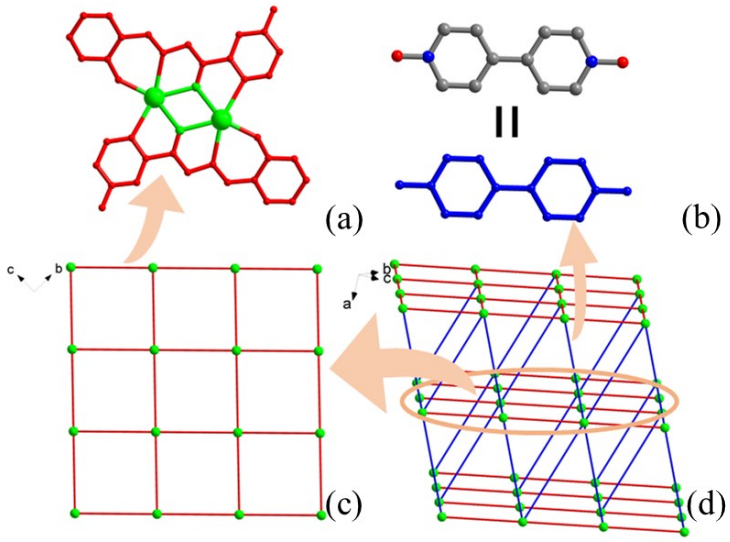

Fig. S1. The 8-connected dimeric Dy_2 subunit and 2-connected L^{2-} ligand (a), the 2-connected bridging ligand of bpdo (b), simplified 2D layer (c), and 8-connected 3D topology for **2**.

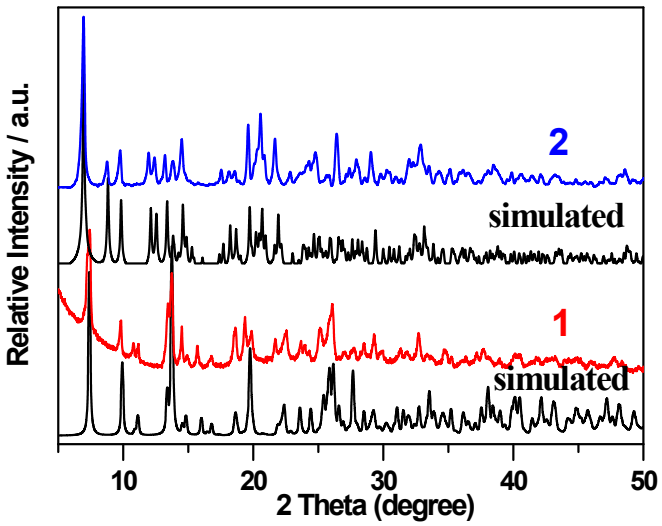

Fig. S2. Powder X-ray diffraction profiles of **1** and **2** together with simulations from the single crystal data.

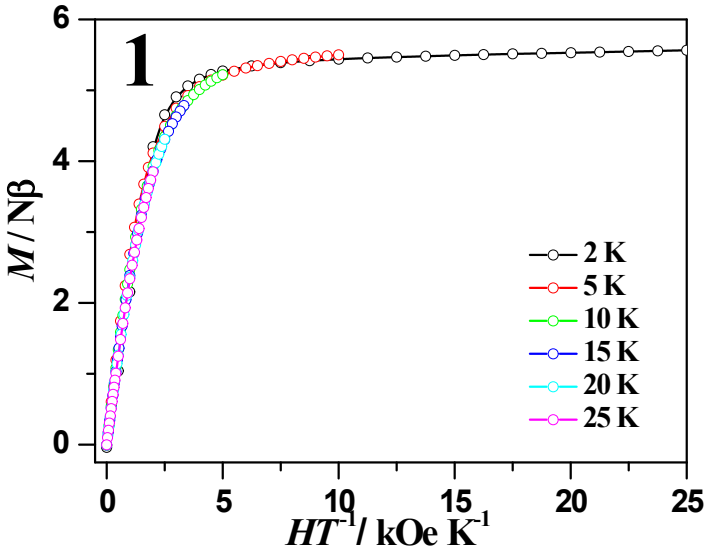

Fig. S3. Plots of *M*-*H* for **1** at 2, 5, 10, 15, 20, and 25 K.

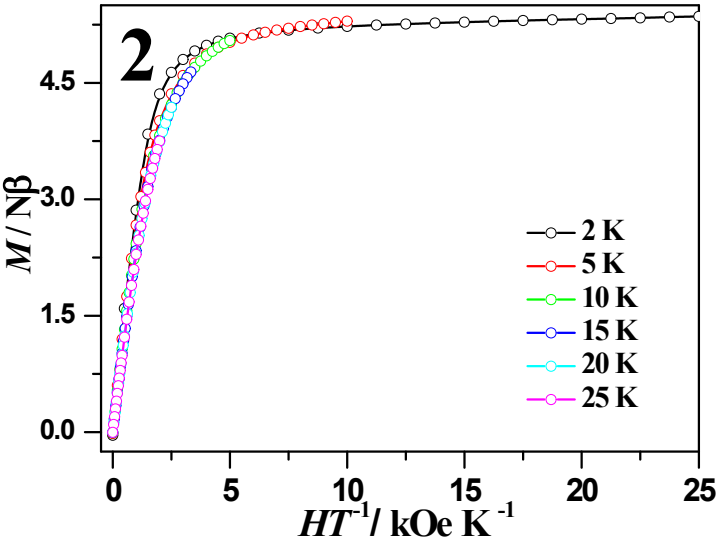

Fig. S4. Plots of *M*-*H* for **2** at 2, 5, 10, 15, 20, and 25 K.

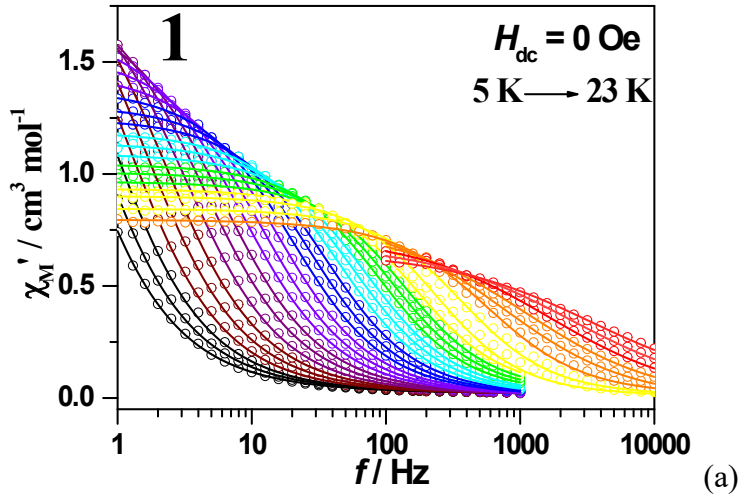

(a)

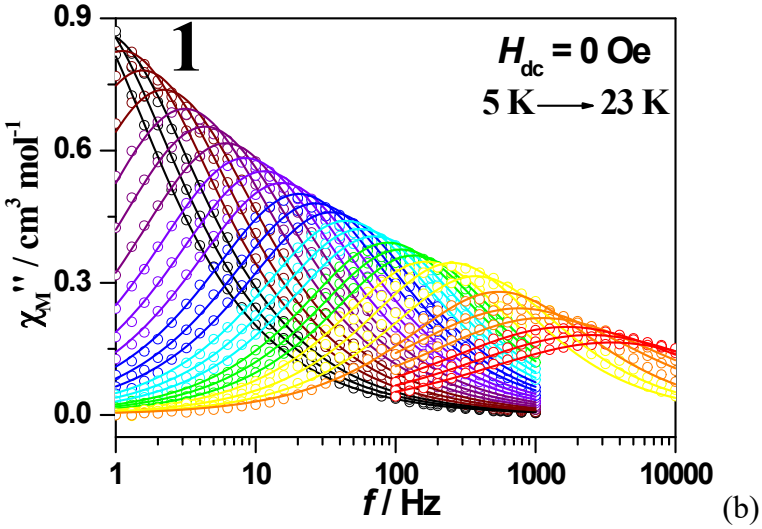

(b)

Fig. S5. Ac-f curves measured under zero dc fields for **1**. Solid lines were fitted using a generalized Debye relaxation model, simultaneously to χ'(*f*) and χ'' (*f*) curves.

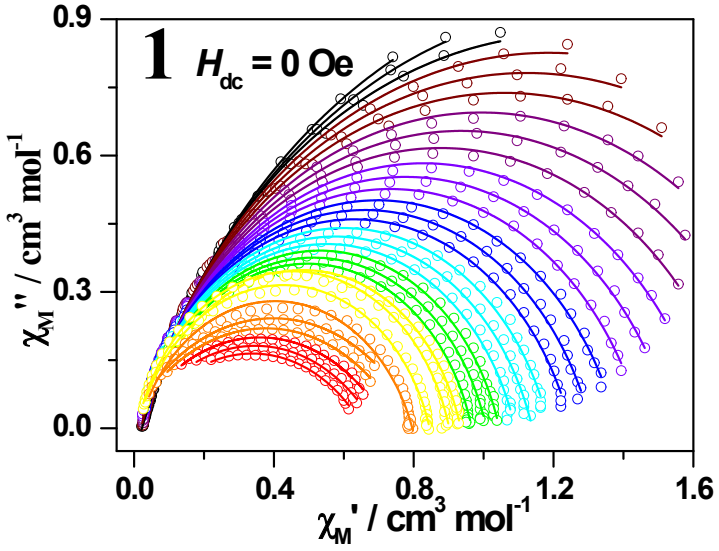

Fig. S6. Cole-cole plots of **1** under zero dc field.

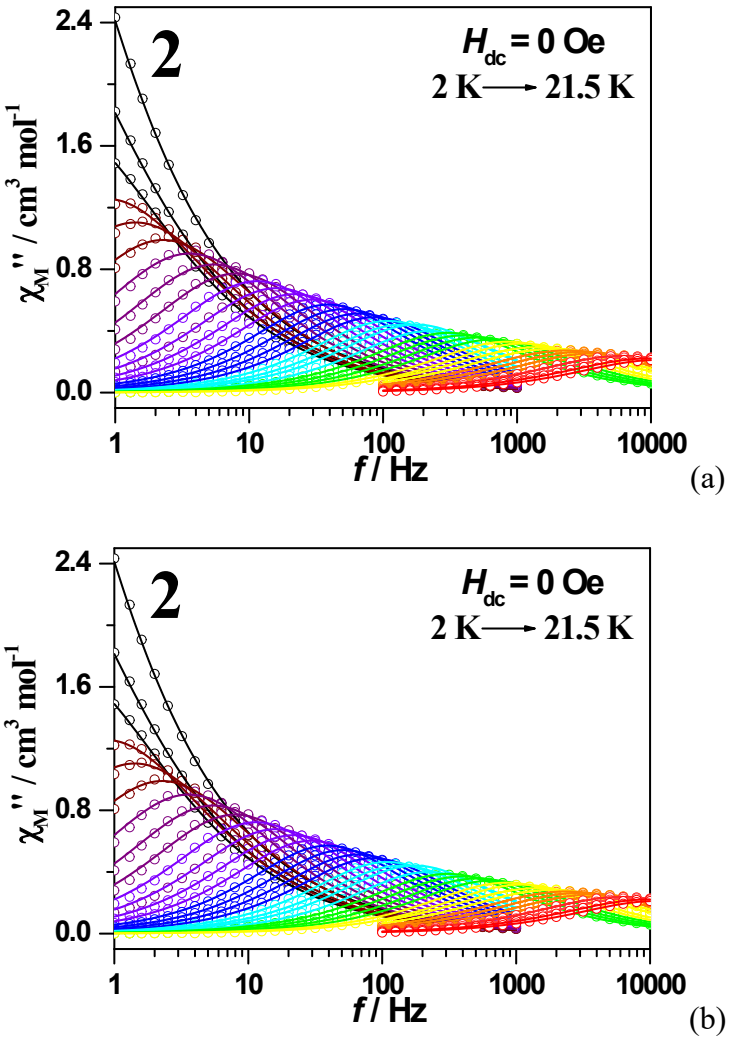

Fig. S7. Ac-f curves measured under zero dc fields for **2**. Solid lines were fitted using a generalized Debye relaxation model, simultaneously to χ' (*f*) and χ'' (*f*) curves.

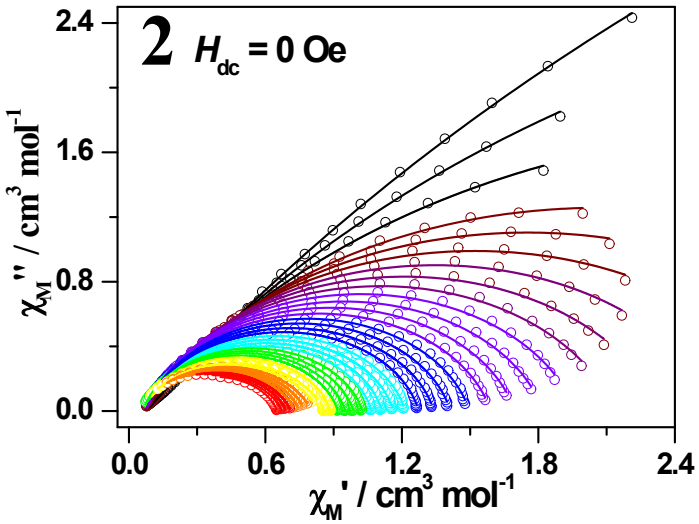

Fig. S8. Cole-cole plots of **2** under zero dc field.

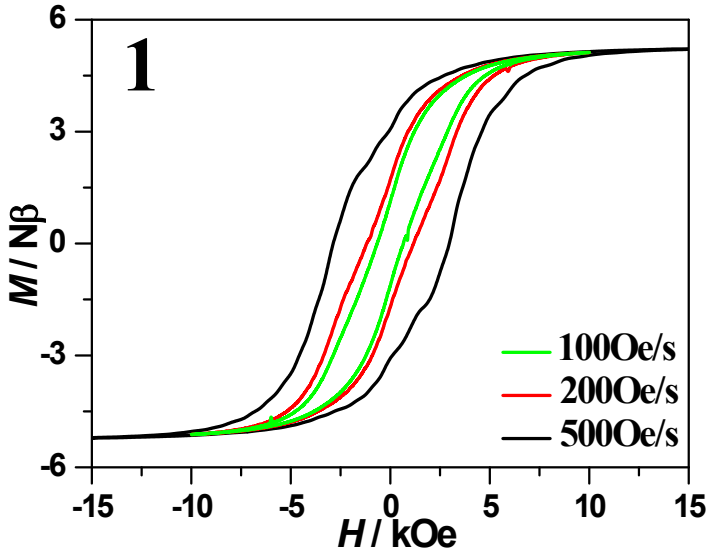

Fig. S9. Hysteresis loop measured with different sweeping rates at 2 K for **1**.

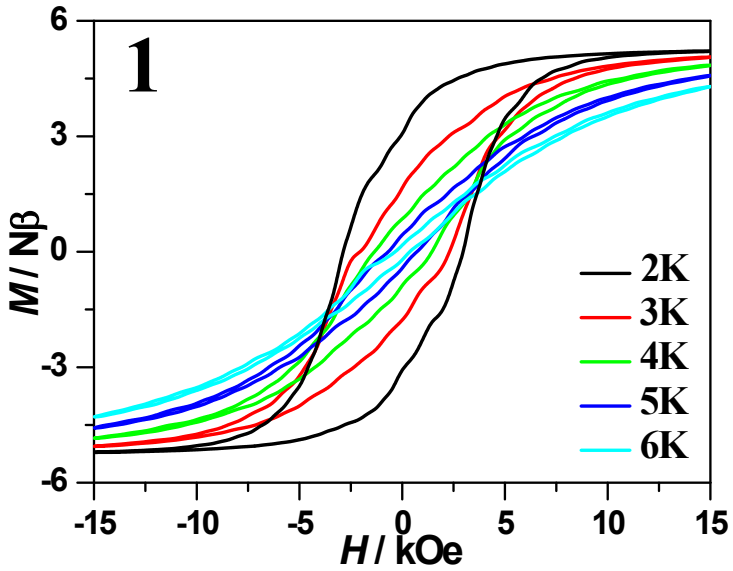

Fig. S10. Hysteresis loop measured at different temperatures with a sweeping rate of 500 Oe/s for **1**.

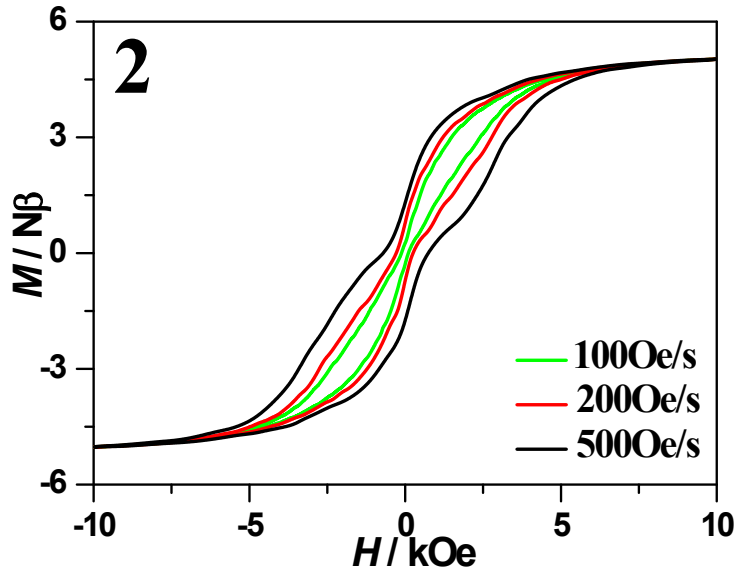

Fig. S11. Hysteresis loop measured with different sweeping rates at 2 K for **2**.

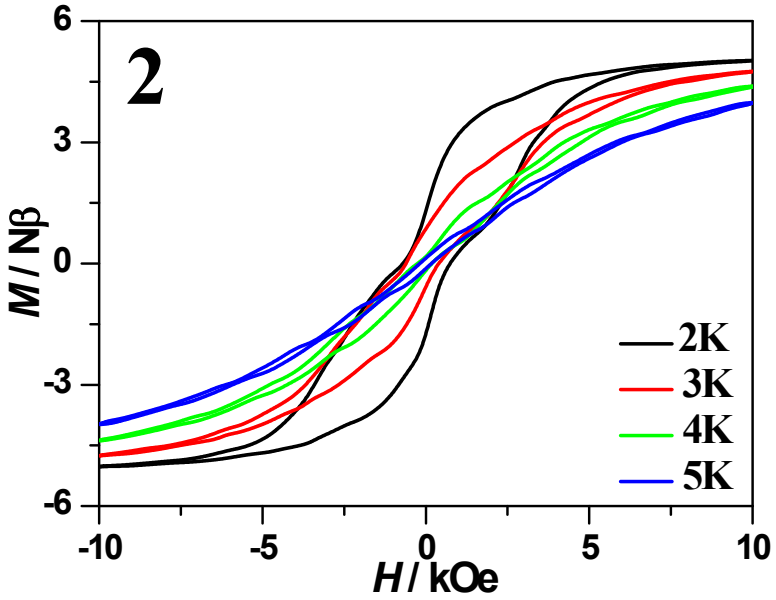

Fig. S12. Hysteresis loop measured at different temperatures with a sweeping rate of 500 Oe/s for **2**.

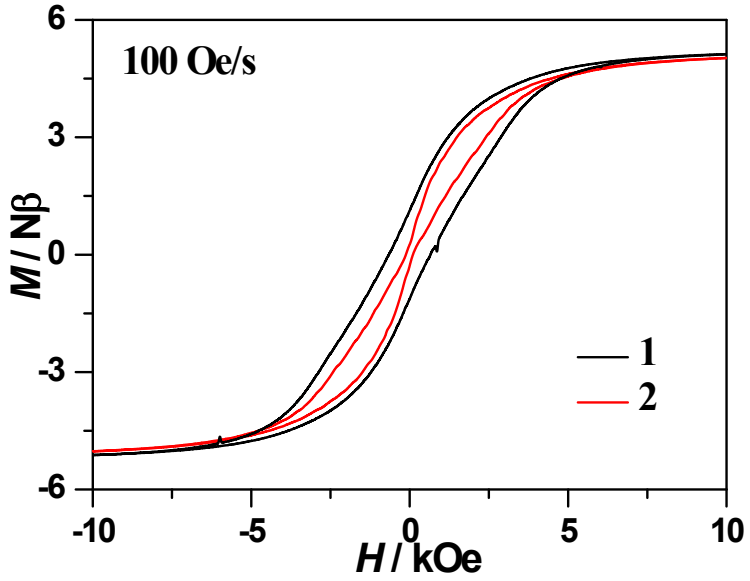

Fig. S13. Hysteresis loop measured at 2 K with a sweeping rate of 100 Oe/s for **1** and **2**.

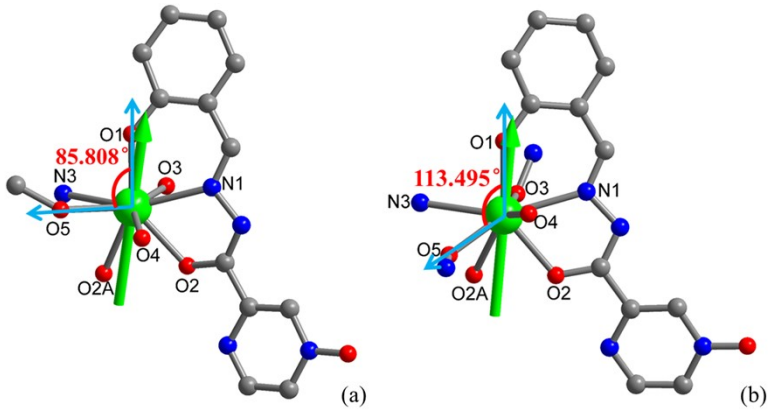

Fig. S14. The bond angles of O1-Dy-O5 around the Dy^{3+} for **1** and **2**.

REFERENCES

1. F. Aquilante, J. Autschbach, R. K. Carlson, L. F. Chibotaru, M. G. Delcey, L. De Vico, I. Fdez Galvan, N. Ferre, L. M. Frutos, L. Gagliardi, M. Garavelli, A. Giussani, C. E. Hoyer, G. Li Manni, H. Lischka, D. Ma, P. A. Malmqvist, T. Muller, A. Nenov, M. Olivucci, T. B. Pedersen, D. Peng, F. Plasser, B. Pritchard, M. Reiher, I. Rivalta, I. Schapiro, J. Segarra-Marti, M. Stenrup, D. G. Truhlar, L. Ungur, A. Valentini, S. Vancoillie, V. Veryazov, V. P. Vysotskiy, O. Weingart, F. Zapata, R. Lindh, Molcas 8: New capabilities for multiconfigurational quantum chemical calculations across the periodic table, *J. Comput. Chem.*, 2016, **37**, 506-541.
2. L. F. Chibotaru, L. Ungur, C. Aronica, H. Elmoll, G. Pilet, D. Luneau, Structure, magnetism and theoretical study of mixed-valent $Co^{II}_3Co^{III}_4$ heptanuclear wheel: Lack of SMM behaviour despite negative magnetic anisotropy, *J. Am. Chem. Soc.*, 2008, **130**, 12445-12455.